Coupled quantum treatment of vibrationally inelastic and vibronic charge transfer in proton-O_2 collisions

F. A. Gianturco
Department of Chemistry, The University of Rome, Città Universitaria, 00185 Rome, Italy

Amedeo Palma, E. Semprini, and F. Stefani
Instituto Teoria e Structure Elettronica, Consiglio Nazionale delle Ricerche, Area della Ricerca di Roma, Monterotondo Scalo, 00016 Rome, Italy

Michael Baer
Department of Theoretical Physics and Applied Mathematics, Soreq Nuclear Research Centre, Yavne 70600 Israel
(Received 16 February 1990)

A three-dimensional quantum-mechanical study of vibrational, state-resolved differential cross sections (DCS) for the direct inelastic and for the charge-transfer scattering channels has been carried out for the $H^+ + O_2$ system. The collision energy considered was $E_{c.m.} = 23.0$ eV, which is the same as that examined by Noll and Toennies in their experiments [J. Chem. Phys. **85**, 3313 (1986)]. The scattering treatment employed was the charge-transfer infinite-order sudden approximation (CT IOSA) with the vibrational states correctly expanded over the relevant adiabatic basis for each of the two electronic channels. The state-to-state DCS are found to follow closely the behavior of the experimental quantities, both in the inelastic and the charge-transfer channels. Moreover, a careful comparison between the measured relative probabilities and computed values allows us to test in minute detail the efficiency of the scattering model and the reliability of the potential-energy surfaces employed. It is found that vibrational energy transfer is overestimated in the vibrational inelastic channels while in the charge-transfer inelastic channels the same energy transfer is slightly underestimated by the calculations. The total flux distribution, however, is found to be in very good accord with experiments. Angular distributions are also well reproduced both by the DCS and by the average energy-transfer values. The study of some of the CT IOSA quantities also allows us to establish clearly the importance of nonadiabatic transitions in enhancing vibrational inelasticity in the present system.

I. INTRODUCTION

The investigation of the dynamics of proton-molecule vibrational interactions at low collision energies, 10 eV $\leq E \leq$ 50 eV, has recently received considerable attention from the experimental viewpoint, where measurements of vibrationally resolved charge-transfer spectra have been carried out for a number of different systems and over a wide range of scattering angles and relative energies.[1-5]

Charge-transfer collisions in the low-energy regime are a fairly recent discovery and involve phenomena of great fundamental and practical interest, in connection with properties of atomic and molecular plasmas, fusion reactor technology, and upper-atmosphere processes. The more recent results from molecular-beam experiments help to elucidate the microscopic mechanisms involved in the simpler rotovibrationally inelastic collisions, and contribute to a better understanding of the general field of nonadiabatic charge transfer vibronic-coupling phenomena during collisions.[6]

These processes belong to the broader class of scattering events that involve transitions between two or more potential-energy surfaces (PES's). Such transitions tend to occur in well-defined regions of configuration space where diabatic potential surfaces cross each other and the Born-Oppenheimer (BO) approximation for the nuclear motion breaks down.

At the present time, however, rather little is known about the detailed dynamics of such "reactive" processes whenever one of the partners is a molecule. This is due to the increased difficulty of collecting experimental information on the wealth of state-to-state inelastic channels which become accessible in a molecular system, as opposed to the simpler atom-ion cases.[7] Moreover, the corresponding theoretical treatment becomes also more complicated than in those molecular cases where only one adiabatic PES is involved in the collisional events. A reliable knowledge of the different PES is in fact necessary over a broad range of relative nuclear geometries, and the corresponding dynamics must now follow all these surfaces. In addition, it must adequately account for all the possible transitions in the whole molecular configuration space from one surface to the next, and must contain the knowledge of the various nonadiabatic couplings that control the corresponding transition probabilities.

Because of this great increase in complexity, most theoretical treatments have relied on some semiclassical approach,[8] be it either the so-called Bauer, Fisher, and Gilmore (BFG) approach based on the construction of diabatic molecular states that interact at crossing points,[9]

or the trajectory-surface-hopping model (TSHM), first suggested by Bjerre and Nikitin,[10] and used already extensively on various systems.[11]

The present study was motivated by the specific series of experiments on the oxygen molecule, whereby vibrationally resolved differential cross sections were measured both for the inelastic and charge-transfer channels:[1,3]

$$H^+ + O_2(v_i=0) \rightarrow \begin{cases} H^+ + O_2(v_f), & \Delta E_0 = 0 \text{ eV} \quad (1a) \\ H^+O_2^+(v_f), & \Delta E_0 = 1.55 \text{ eV} . \quad (1b) \end{cases}$$

The experiments were carried out at a c.m. energy of 23.0 eV by measuring the product H (H^+) atom energy distributions in the range $0° \leq \theta \leq 11°$. They show a strong dependence of the distribution of vibrational transition probabilities $P_{0 \rightarrow v_f}$ of both channels on the scattering angle, and quite a marked departure from the expected Franck-Condon (FC) distribution, which would be peaked at $v_f = 1$.

A similar set of data had been collected by the same experimental group for the $H^+ + H_2$ system,[4] and in that case calculations were carried out quite successfully within a quantum-mechanical framework[12] by using a previously computed diatomic-in-molecules (DIM) set of potential surfaces.[13] The present system, however, is much more complicated than the two-electron case just discussed, and therefore several earlier studies simply were limited to a qualitative interpretation of the experiments.[3,14]

The more recent availability of a full PES for both the direct inelastic channel and the charge-transfer channel involved in Eq. (1) (Ref. 15) has prompted us to look once more at this system and to apply a fully dynamical approach which would also take into consideration the nonadiabatic coupling between the relevant potential surfaces. The following section therefore describes how the DIM interaction of Ref. 15 has been employed in the present calculations, and how it compared with other descriptions of the hypersurfaces. Section III will discuss in detail the quantum treatment of the coupled dynamics, while Sec. IV will present the computed results and their comparison with experiments.

II. THE POTENTIAL HYPERSURFACES

A. The DIM interaction

The application of the DIM method to a system that contains more than one non-*S*-state atom becomes rapidly rather complicated because of the large dimensions of realistic DIM matrices and because of the large amount of input data required. In order to retain the main advantages of such a modeling of the interactions, i.e., small matrix dimensions and rapid computations of each of the needed points in the full configuration space, it was decided[15] to substantially restrict the diatomic basis set and to introduce empirical adjustments of selected excited-state input data in order to compensate for the previous restriction, and to fit existing *ab initio* data for some of the nuclear geometries coming from multireference configuration-interaction (single+double) [MRCI(SD)] calculations via a triple-zeta+diffuse+polarization (TZDP) basis set.[16] The chosen DIM basis structures corresponded to the two energetically lowest channels:

$$O(^3P_g) + O(^3P_g) + H^+ , \quad (2a)$$

$$O^+(^4S_u) + O(^3P_g) + H(^2S_g) . \quad (2b)$$

Thus, when constructing all possible triplet-state functions from the above structures, one arrives at 8 A'' and 13 A' functions. The resultant Hamiltonian matrix size is therefore 21×21, and the construction of the corresponding matrix elements has been already described elsewhere.[15,17] The corresponding diatomic fragments were 4 for OH^+, 4 for the OH,O_2^+, and 6 for O_2 and their potential-energy curves were represented as spline interpolations or as generalized Morse fits.

The final potential-energy surfaces selected for the present calculations involved the lowest two adiabatic PES's produced by the DIM modeling of the interaction.

In the more general C_s geometries of the three-atom interactions, they correspond to the $1\,^3A''$ and the $2\,^3A''$ surfaces, while they become $1\,^3B_2$ and $1\,^3A_2$ in the C_{2v} calculation, and $1\,^3\Sigma^-$, and $1\,^3\Pi$ in the $C_{\infty v}$ geometry.

It is interesting to note here that a different type of model calculation on the same system had been carried out by Grimbert *et al.*,[18] where the authors devised an effective model-potential approach to describe the low-lying $^3A''$ state of the $H^+ + O_2$ system.

A comparison[15] of their model adiabatic states with those given by the DIM calculations gave a general qualitative agreement between the results from the two different methods, although the effective-potential curves, at fixed O_2 geometry, exhibited a stronger angular (orientational) dependence than the DIM curves. Such a difference will have some specific effect, naturally, on the outcome of dynamical calculations, and will be further discussed in Sec. IV.

The additional advantage of the DIM modeling of the interaction appears clearly when nonadiabatic-coupling terms need to be evaluated between the PES's. In this case, one can show[19] that all the relevant coupling derivatives with respect to the three internal nuclear coordinates (R, r, and γ) can be obtained via a generalization of the Hellman-Feynman theorem using the corresponding eigenvalues of the full DIM Hamiltonian and the eigenfunctions of the states that one intends to couple.[20] A detailed description of such coupling terms and of their dependence on the internal coordinates above has already been reported elsewhere[20] and will not be repeated here.

In the case of the model potential which generated diabatic states, on the other hand, the nonadiabatic couplings were given by the off-diagonal terms of the model electronic Hamiltonian,[18] and they showed that the interactions between the repulsive $H+O_2^+(X\,^2\Pi_g)$ state and higher-lying charge-exchange states also appear to be nonnegligible within their effective-potential models. Although also present in our DIM calculations, they have not been considered as important in the following calculations, nor were they included in the quantum treatment of the collision that employed the latter diabatic states.[21] The physical reasons for this exclusion will become evi-

dent during the discussion of the results, as they hinge on the found dominance of the first (outer) crossing region in inducing vibrationally inelastic processes in either of the channels considered by the experiments.

It is not obvious, however, how to compare directly the specific behavior of the nonadiabatic couplings as given by the two different model calculations of Ref. 15 and 18: one can only say at this point that both models suggest only a weak dependence on γ for the H_{12} or Δ_{12} coupling elements in the radial regions outside the crossing, with a marked increase within the relative distances between that crossing and turning point. Moreover, all couplings appear to peak at the R values around the crossing when the adiabatic curves are considered, and this "localization" of nonadiabatic effects will be further discussed when analyzing the results from the scattering calculations.

B. The transformation to diabatic states

Although in principle all the necessary ingredients to treat the dynamical problem have been obtained within the DIM model, one knows that the direct calculation within the adiabatic framework is fraught with several severe numerical instability problems due to the special behavior of the nonadiabatic couplings with respect to the collision coordinates. Thus, one is forced to apply a series of adiabatic-to-diabatic transformations to eliminate the erroneous behavior of the couplings and to obtain treatable coupled equations with diabatic states.[22] Since the two representations contain in principle the same information, the solutions and transition probabilities are identical, irrespective of the representation used.

The procedure that follows was originally suggested for the atom-atom case;[23] it was then extended to the atom-molecule case,[22] and then further applied to a generalized set of coordinates.[24]

Following the usual BO formulations, the wave function depending on electronic ξ and nuclear $\mathbf{R}$ coordinates can be expanded over the two states involved in the process as

$$\Psi(\xi,\mathbf{R})=\sum_{i=1}^{2}\phi_i(\xi;\mathbf{R})\chi_i(\mathbf{R}) , \tag{3}$$

where the ϕ_i are eigenfunctions of the fixed-nuclei Hamiltonian $\mathcal{H}_{\rm el}$. Standard substitution into the Schrödinger equation for the total Hamiltonian

$$\mathcal{H}_{\rm tot}=\mathcal{H}_{\rm el}+\hat{T}_R , \tag{4}$$

where $\hat{T}_R$ now stands for the nuclear kinetic energy operator, leads to the usual definition of two adiabatic surfaces $V_i(R,r,\gamma)$ corresponding to the two states involved. The variables are now the collision coordinate $\mathbf{R}$, the internal coordinate $\mathbf{r}$ and $\gamma=\cos^{-1}(\hat{R}\cdot\hat{\mathbf{r}})$, the internal orientation angle. The corresponding nonadiabatic 2×2 coupling matrices $\underline{\tau}^{(1)}$ and $\underline{\tau}^{(2)}$ contain the following elements:

$$\tau_{ij}^{(1)}=\langle\phi_j|\nabla\phi_i\rangle , \tag{5a}$$

$$\tau_{ij}^{(2)}=\langle\phi_j|\nabla^2\phi_i\rangle . \tag{5b}$$

The derivative operator vector ∇ is given by

$$\nabla=\left[\frac{\partial}{\partial R},\frac{\partial}{\partial r},\frac{1}{a}\frac{\partial}{\partial\gamma}\right] , \tag{6}$$

where all the internal coordinates have been defined before and the coefficient a can be shown[25] to be

$$a=\frac{rR}{(R^2+r^2)^{1/2}} . \tag{7}$$

The singularities of the nonadiabatic-coupling terms in the asymptotic regions and their abrupt changes within definite regions of configuration space introduce severe difficulties in the search for linearly independent, numerically stable solutions of the ensuing coupled equations. They can be avoided if one transforms the nuclear functions into another set of wave functions:

$$\chi=\underline{\mathcal{A}}\eta , \tag{8}$$

where the orthogonal matrix $\underline{\mathcal{A}}$ is chosen so as to fulfill the following vector equation:

$$\nabla\underline{\mathcal{A}}+\underline{\tau}^{(1)}\underline{\mathcal{A}}=0 . \tag{9a}$$

By employing completeness relations one can show that $\underline{\mathcal{A}}$ also satisfies the following equation:

$$\nabla^2\underline{\mathcal{A}}+2\underline{\tau}^{(1)}\cdot\underline{\mathcal{A}}+\underline{\tau}^{(2)}\underline{\mathcal{A}}=0 . \tag{9b}$$

Under the above conditions, one can show[26] that the Schrödinger equation governing the nuclear motion for the auxiliary functions defined in Eq. (8) simplifies greatly and can be written as

$$\nabla^2\eta-\frac{2\mu}{\hbar^2}(\underline{W}-E)\eta , \tag{10}$$

where $\underline{W}$ is now the desired diabatic potential matrix, which is defined in terms of the either adiabatic potentials V_{ij}, which follow from the DIM results

$$\underline{W}=\underline{\mathcal{A}}^*\underline{V}\underline{\mathcal{A}} . \tag{11}$$

Thus, the nonadiabatic-coupling terms between adiabatic states are now shifted in the full potential matrix between diabatic states. Also note that the coupling elements of Eq. (5b) have been eliminated by the unitary transformation (8) and therefore do not appear any more in Eq. (10).

In the present case only two adiabatic surfaces have been considered to be important to study the process in question. Thus, the orthogonal matrix $\underline{\mathcal{A}}$ can be written[22] in the familiar form

$$\underline{\mathcal{A}}=\begin{bmatrix}\cos\alpha & \sin\alpha\\ -\sin\alpha & \cos\alpha\end{bmatrix} , \tag{12}$$

and the transformation angle α is a function of our three internal variables[25,26]

$$\alpha(R,r,\gamma)=\alpha_0+\int_{r_0}^{r}\tau_r^{(1)}(R,r,\gamma)dr+\int_{R_i}^{R}\tau_R^{(1)}(R,r_0,\gamma)dR+\int_{\gamma_0}^{\gamma}\tau_\gamma^{(1)}(R_0,r_0,\gamma)d\gamma , \tag{13}$$

where the ranges of integration for each of the above terms will be discussed below, and each of the coupling

terms in the integrands are elements of the $\underline{\tau}^{(1)}$ matrix defined in Eq. (5a) with respect to each of the internal variables of our problem.

Once the transformation angle is known for a given set of nuclear variables, then the elements of the diabatic matrix are easily obtained for that geometry [see Eq. (11)]:

$$W_1(R,r,\gamma)= V_1(R,r,\gamma)\cos^2\alpha(R,r,\gamma) + V_2(R,r,\gamma)\sin^2\alpha(R,r,\gamma) ; \quad (14a)$$

$$W_2(R,r,\gamma)= V_1(R,r,\gamma)\sin^2\alpha(R,r,\gamma) + V_2(R,r,\gamma)\cos^2\alpha(R,r,\gamma) ; \quad (14b)$$

$$W_{12}=W_{21}(R,r,\gamma)=\tfrac{1}{2}(V_2-V_1)\sin^2\alpha(R,\gamma,r) . \quad (14c)$$

For each of the values of the relative orientation γ and the molecular coordinate r, the transformation angle can be seen to become a step function as R goes to ∞, since the nonadiabatic-coupling terms become a δ function.[25] In other words, the correct asymptotic behavior of α determines whether we have reached the correct asymptotic limit of the interaction as the H^+ (or H) atom is moved to infinity, and the corresponding diatomic curves for either O_2 or O_2^+ are correctly described by W_1 and W_2. The internal coordinate value that will distinguish between the two situations will be r_s, the intersection point between the shifted diatomic potentials of O_2 and O_2^+. In the present case r_s was given by $1.6a_0$, rather close to the actual experimental value.[27]

It was also found to be expedient to carry out the dynamical integration by performing a further transformation of the diabatic potentials in such a way as to minimize the off-diagonal term.[25] In other words, to select a simple path for $r(R)$ in such a way as to have $W_{12}(r(R),R)\approx 0$, thereby choosing among the many possible transformations to diabatic basis the one which stays the closest to the original adiabatic representation. In the present case, as tested previously,[12,28] it was found convenient to select a straight line along R with a constant r value, chosen to be a minimum energy path with $r\sim 1.15$ Å.

The behavior of the transformation angle as a function of R and r is shown in Fig. 1, where one particular γ value is chosen, i.e., the $\gamma=45°$, corresponding to the angular region of strongest coupling[20] between the two adiabatic states. One clearly sees there that the V_1 and V_2 potentials are indeed strongly mixed at small R values and as r goes through the crossing point r_s ($1.6a_0$). On the other hand, as R goes beyond the outer curve crossing ($\sim 4.8a_0$), the shape of the transformation angle becomes more and more like the correct step-function behavior. We also found that such general behavior was common to several γ values and that the general shape of the α angle was slowly changing with orientation. As a consequence of these findings, we decided to follow previous procedures,[12,28] and treated $\alpha(R,r)$ as independent of γ in the actual calculation. The consequences of this choice will be further discussed when examining the comparison of the present results with the experiments.

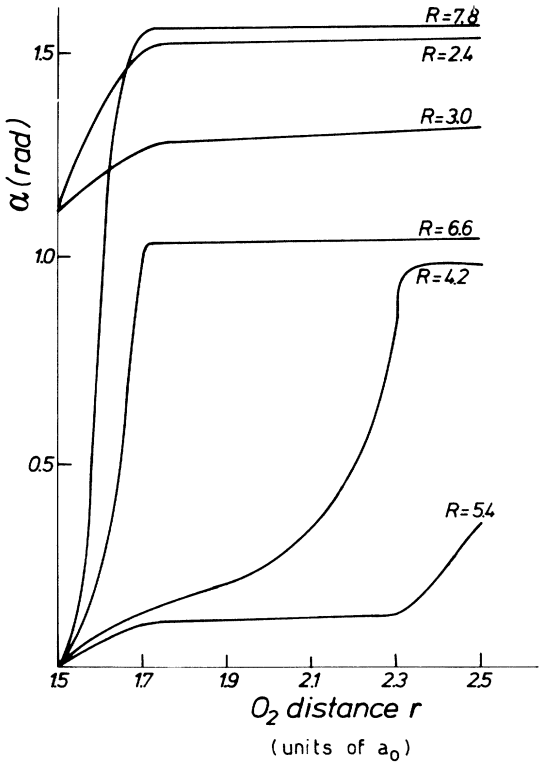

FIG. 1. The transformation angle α as a function of the molecular coordinate r and of the collision coordinate R. The orientation angle γ was chosen to be 45°. All coordinate values in a.u. and α values in rad.

III. THE QUANTUM DYNAMICS

As mentioned in the Introduction, the combined complexity of the additional molecular degrees of freedom and of the multicurve aspects of the interaction hypersurfaces has long prevented the acquisition of quantitative knowledge of the detailed dynamics which controls inelastic charge-exchange collisions in molecular systems. Thus, most of the computational approaches have relied on a classical treatment of the collision trajectories, while preserving the quantal nature of the molecular internal motion and the interstate couplings.[8,13] In the present case we have decided instead to treat both internal motion and collisional motion of equal footing and to formulate their equations within a quantum framework. The only simplification that we have introduced is the one dictated by the physics of the collisional events, namely, we have taken advantage of the fact that the relative collision energy allows us to separate rotational from vibrational motions. At the present energy, in fact, the expected time of interaction between colliding partners is of the order of a few vibrations[3] and is therefore much shorter than a molecular rotation, if we consider the target molecule to be at a rotational temperature of a few K.[1] Thus, one can say that the electronic excitation that takes place during the charge-transfer process effectively couples dynamically with the vibra-

tional motion but not with the rotational motion of the target. In other words, the full rotovibronic problem is reduced, due to the above time-scale considerations, to a different vibronic problem for each of the relative orientations between the H^+ (H) projectile and the O_2 (O_2^+) target, which are chosen to generate the diabatic potential matrix.

A. The coupled equations

The previous discussion simply amounts to the treatment of rotational degrees of freedom in a way that is decoupled from the dynamics of the relative motion, while the vibrations are taken to be coupled to the electronic excitation during the collisional event. When motion along only one potential-energy surface is considered, the approach is usually termed the vibrational coupled-channel plus rotational infinite-order sudden approximation (VCC RIOSA) of the scattering process.[29] Moreover, one can simplify further the problem by not only treating the purely adiabatic part of the collision [thereby setting to zero the nonadiabatic coupling terms of Eq. (5)], but by considering only the rotational motion during the vibrationally elastic collisions. Our previous calculations along these lines[30] have indeed shown that partial, inelastic integral cross sections are fairly small for the present system, and therefore it makes physical sense to treat the full vibronic coupling within the rotational decoupling discussed above while still using all the necessary potential-energy surfaces and nonadiabatic coupling. This approach is called the change-transfer infinite-order sudden approximation (CT IOSA) (Refs. 12 and 28) treatment of the dynamics.

The corresponding coupled equations, obtained by considering only the two lowest PES's of the DIM calculations discussed earlier, now take the following familiar form,[28] by using atomic units throughout:

$$\left[-\frac{1}{2\mu}\left[\frac{\partial^2}{\partial R^2}+\frac{\partial^2}{\partial r^2}\right]+W_{11}+\frac{l(l+1)}{2\mu R^2}-E\right]\psi_1(R,r,\gamma)+W_{12}\psi_2(R,r,\gamma)=0\ ; \tag{15a}$$

$$\left[-\frac{1}{2\mu}\left[\frac{\partial^2}{\partial R^2}+\frac{\partial^2}{\partial r^2}\right]+W_{22}+\frac{l(l+1)}{2\mu R^2}-E\right]\psi_2(R,r,\gamma)+W_{12}\psi_1(R,r,\gamma)=0\ . \tag{15b}$$

The transformation angle α can now be computed for each equation by keeping γ fixed. Thus Eq. (13) becomes now a simpler relation in which the last term on its right-hand side (rhs) can be added to α_0 to form a new constant, $\bar{\alpha}(\gamma)$, for each pair of IOSA equations:

$$\alpha^{\mathrm{IOSA}}(R,r;\gamma)=\bar{\alpha}(\gamma)+\int_{r_0}^{r}\tau_r^{(1)}(R,r,\gamma)dr+\int_{R_i}^{R}\tau_R^{(1)}(R,r_0,\gamma)dR\ . \tag{16}$$

The nonadiabatic couplings $\tau_p^{(1)}$ can be obtained directly from the DIM calculations by using the Hellman-Feynman theorem and the full DIM matrix over the states discussed earlier:[20]

$$\tau_p^{(1)}=\frac{\mathbf{A}_2^{*}(\partial\underline{H}/\partial p)\mathbf{A}_1}{V_2-V_1},\quad p=R,r,\gamma \tag{17}$$

where $\mathbf{A}_1$ and $\mathbf{A}_2$ are the eigenvectors associated with the chosen V_1 and V_2 lowest eigenvalues of the Hamiltonian DIM matrix $\underline{H}$.

The target vibrational states for either O_2 by O_2^+ were obtained within a molecular adiabatic picture, namely at selected values (see below) of the collision coordinate R. The vibrational bound states in the molecular coordinate r were obtained numerically by using the W_{11} and W_{22} potential functions. Each set was then used to expand either the ψ_1 or the ψ_2 wave function to obtain the corresponding coupled equations for the vibronic process given by Eq. (15). The numerical details of this approach will be discussed below in Sec. III C.

B. The computed IOSA observables

Since the final outcome of solving the CT IOSA equations is the corresponding angle-dependent S-matrix elements, there are several useful quantities which can be obtained from the calculations and either compared directly with dynamical observables or employed to further understand the forces at play in the vibronic collisional processes.

Thus, one can rather straightforwardly write down the partial differential cross sections:

$$\frac{d\sigma^q(v_i\rightarrow v_f)}{d\Omega}=\frac{1}{8\kappa_{v_i}^2}\sum_{l,l'}(2l+1)(2l'+1)P_l(\cos\theta)\times P_{l'}(\cos\theta)\int_{-1}^{1}d(\cos\gamma)S^q(E,\gamma,l,v_i,v_f)S^{q*}(E,\gamma,l',v_i,v_f) \tag{18}$$

where E is the total collisional energy, v_i and v_f are the two vibrational states involved in the transition, κ_{v_i} is the initial wave vector, and the S^q's are the S-matrix elements yielded by the previous calculations.

The index q designates either the vibrationally excited (VE) direct process or the charge-transfer channel (CT).

Another quantity that is obviously of value when discussing the experimental results is the partial integral cross section for either of the above channels:

$$\sigma^q(v_i \rightarrow v_f|E)=\frac{\pi}{2\kappa^2_{v_i}} \sum_l (2l+1) \int_{-1}^{1} d(\cos\gamma)|S^q(E,\gamma,l,v_i,v_f)|^2 \ . \tag{19}$$

From the experimental transition probabilities $P_{0\rightarrow v'}$ as given by the time-of-flight spectra,[1] one can also determine the average vibrational-energy transfers in both channels as a function of the scattering angle:

$$\Delta E^q_{\text{vib}} = \sum_{v' \neq 0}^{\infty} P^q_{0\rightarrow v'} \Delta E(0 \rightarrow v') \ , \tag{20}$$

where the superscript q designates again either the VE or the CT channels defined above. Each of the individual probabilities is in turn determined from the state-to-state individual DCS:

$$P^q_{0\rightarrow v'} = \frac{d\sigma^q(0\rightarrow v')}{d\Omega} \Big/ \sum_{v' \neq 0}^{v_{\max}} \frac{d\sigma^q(0\rightarrow v')}{d\Omega} \ , \tag{21}$$

where the normalization is given by the sum of all observed DCS's up to the maximum experimentally available vibrational state of the O_2 or O_2^+ targets, $v_{\max}$. The observed values for the above quantities were given in Ref. 1 and will be compared with our calculated values in the following section.

In order to gain some further insight into the specific microscopic mechanisms, it is of interest to also make use of the following functions that are produced by the IOSA calculations, albeit not as directly observables quantities. One of these is the partial opacity function

$$P^q(E,l|v_i,v_f)=\tfrac{1}{2}\int_{-1}^{1} d(\cos\gamma)|S^q(E,\gamma,l,v_i,v_f)|^2 \ , \tag{22}$$

which defines the relative probability that a given process, labeled by the channel index q, occurs as a function of the impact parameter (related to each contributing orbital angular-momentum quantum number l) of the initial vibrational state v_i and of the final vibrational state v_f.[12,28]

Naturally, one can also define the corresponding total quantity summed over all final vibrational states, i.e., the opacity sum:

$$P^q_{v_i}(E,l)=\sum_{v_f} P^q(E,l,|v_i,v_f) \ . \tag{23}$$

Moreover, the use of the IOSA scheme makes it possible to define another cross section that explicitly depends on the orientation angle γ and on the two vibrational states involved:

$$\sigma^q_{v_i\rightarrow v_f}(\gamma)=\frac{\pi}{\kappa^2_{v_i}} \sum_l (2l+1)|S^q(E,\gamma,l,v_i,v_f)|^2 \ . \tag{24}$$

Such a quantity provides specific information about the steric effect of the vibrational and vibronic inelastic processes, i.e., a more transparent relation between features of the involved PES's and outcomes of the dynamical calculations.[31]

The corresponding summed quantity is given by

$$\sigma^q_{v_i}(\gamma)=\sum_{v_f} \sigma^q_{v_i\rightarrow v_f}(\gamma) \ , \tag{25}$$

and the average energy transfers can also be defined in a γ-dependent form:

$$\Delta E^q(\gamma)=\sum_{v_f \neq 0} \sigma^q_{0\rightarrow v_f}(\gamma)\Delta E(0\rightarrow v_f) \times \left[\sum_{v_f \neq 0} \sigma^q_{0\rightarrow v_f}(\gamma)\right]^{-1} \ , \tag{26}$$

where, as before, $\Delta E(0\rightarrow v_f)$ corresponds to the energy difference between the $|v_f\rangle$ and the $|0\rangle$ vibrational levels.

All the above quantities have been computed for the present system and will be compared with the experimental findings in the next section.

C. Numerical details

All calculations, in order to correspond as best as possible to the experimental conditions, were carried out for an initial translational energy of $E_{\text{c.m.}}=23.0$ eV ($E_{\text{lab}}=23.7$ eV) and for $v_i=0$. For solving the coupled equations the total number of adiabatic vibrational states was found to be sufficiently converged when equal to 40, with 20 states included for each surface.

The effects from the inclusion of additional vibrational states were not looked at systematically. However, since previous calculations[21] on the same systems included a smaller number of vibrational states and found no effect on their converged results, no further enlargement of the basis set was considered to be necessary. The coupled equations were solved for 16 equally spaced values of γ and the number of partial waves included was extended beyond $l=410$ in order to ensure the numerical convergence of the partial and total opacity functions. The r integration ranged over the interval of $1.5a_0 \leq r \leq 4.0a_0$ and the R integration went over the interval of $0.8a_0 \leq R \leq 9.0a_0$, using a 2D-spline interpolation of the $\{r,R\}$ potential data for each of the considered γ values. A total number of 96,000 data points were employed in the $\{r,R,\gamma\}$ space of variables during the numerical integration. Considerable care needed to be used in the choice of the initial and final values in the collision variable for the integration. It was found that one could not start at $R=0$ because of numerical instabilities of the solutions in the region of strong coupling, a feature that makes the opacity values less accurate at small l. However, as all the experimental data were concerned with the forward scattering cross sections, this inaccuracy was not considered to be of importance.

The computed DCS's also showed considerable undulatory structures as a function of $\theta_{\text{c.m.}}$ due to various types of quantum interference and fast oscillation effects. As the experimental findings are not able to resolve such effects, the computed angular distributions were smoothed as before[12,21] by folding them with a Gaussian distribution:

$$\frac{d\bar{\sigma}}{d\Omega}(\bar{\theta})=\mathfrak{N}\int_{\theta-\Delta\theta}^{\theta+\Delta\theta}\exp\left[-\frac{(\theta-\bar{\theta})^2}{2\sigma_\theta^2}\right]\frac{d\sigma(\theta)}{d\Omega}d\theta\ , \qquad (27)$$

where $\Delta\theta=1°$, $\sigma_\theta=0.33°$, and $\mathfrak{N}$ is a normalization factor.

IV. RESULTS AND DISCUSSION

One attractive feature of the above computational approach is that no adjustments to experimental data has been introduced during its application. The following discussion therefore attempts to look into several aspects of the measurements and to assess through them the specific reliability of each step of this work.

The first quantities which can be obtained and compared with their measured values are the differential cross sections, total and partial, for both the VE and CT channels of the present process. They are shown in Figs. 2 and 3, respectively.

The results for the direct, vibrationally elastic process show several features which agree with experiments (shown in the top part of Fig. 4):

(i) The total cross section correctly diverges as $\theta_{\rm lab}\sim 0°$ and shows a variation of orders of magnitude over the examined angular range, as that shown by the experiments.

(ii) The rainbow angle appears in the same angular region as the experiments, although it is much more marked than the latter and than the previous calculated values.[21] The reduced quenching shown by our calculations may be due to an overall diabatic PES which underestimates the anisotropy and hence the damping induced by it. It gives correctly, however, the effective well depth of the real interaction, as already found by our earlier adiabatic calculations[30] which used the same surfaces.

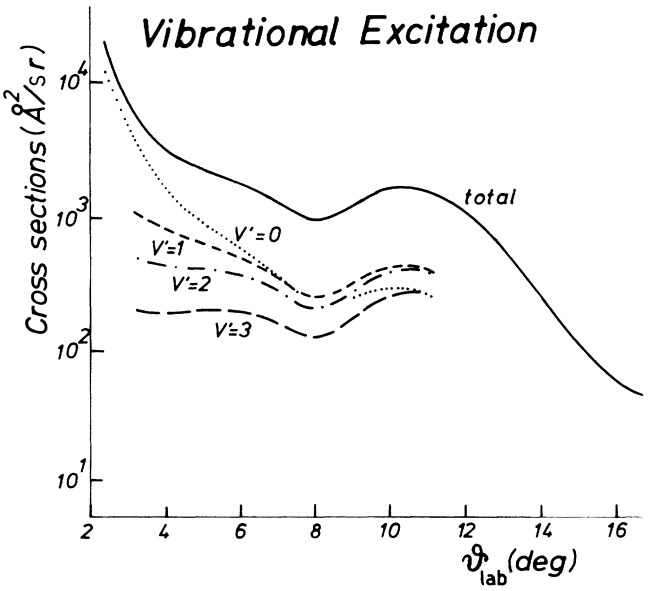

FIG. 2. Computed differential cross sections, partial and total, for the vibrational inelastic, direct channel.

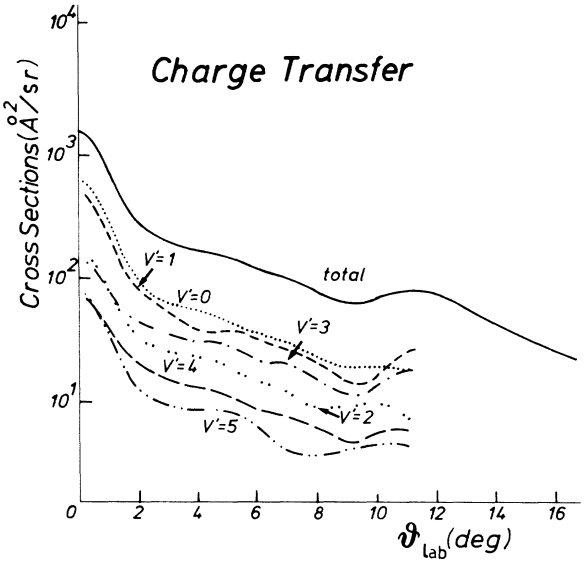

FIG. 3. Same as in Fig. 2 but for the charge-transfer channel.

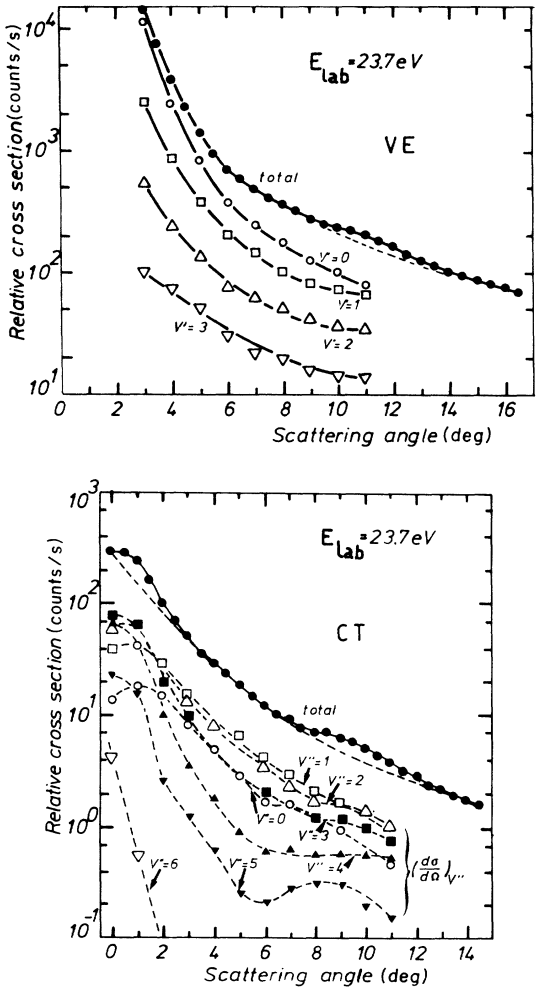

FIG. 4. Experimental data for all the inelastic processes computed in this work. Top part: vibrationally inelastic (VE) channels. Bottom part: inelastic, charge-transfer (CT) channels.

(iii) The individual, partial inelastic DCS's exhibit the same ordering as that shown by the experiments, i.e., they decrease as the final vibrational quantum number v' increases. Moreover, they agree well with experiments in the small-angle region but decrease less than experiments as θ increases. This discrepancy will show its effect more clearly when the relative inelastic probabilities are compared with the measured values, as discussed below.

It is also interesting to note that the previous calculations with a different PES (Ref. 21) exhibited smaller DCS's for the inelastic processes and a much faster intensity decrease, for all of them, as θ_{lab} moved to larger values.

If we now turn to the same quantities for the other available channel, i.e., for the CT process, we still find a generally good agreement between computations and experiments, although the overall picture is now much more complicated. One sees, in fact, in Fig. 3 the behavior of the computed quantities, while the corresponding experiments are shown in the bottom part of Fig. 4.

Many more final states are now excited during the collisional experiment and the present calculations confirm this finding. Moreover, the observed total DCS now tends to a finite value as θ goes to zero (as opposed to the divergent behavior of the one for the previous channel) and the calculated quantity agrees with it rather clearly. The rainbow feature from the calculations is now more markedly quenched than that for the VE channels and agrees better with experiments.

The relative importance of each inelastic process, on the other hand, is different between theory and experiments. Each DCS shows in the latter case a more rapid decrease, as θ_{lab} increases, with respect to the theoretical behavior, and the measured decrease does not follow the sequence of final vibrational levels which is given by the calculations. The total amount of energy transferred during collision is, however, well described by the present theory, as we shall see below.

The detailed behavior of the individual probabilities as a function of scattering angle is also a good tool for further analysis of the performance of the present theoretical model with respect to existing experimental values. This is done by the results shown in Figs. 5 and 6, where the calculations from Ref. 21 are also presented.

The direct VE channels are shown in Fig. 5 together with the published measurements of Ref. 1. One sees immediately that the elastic process is underestimated by theory, which produces for this channel a larger vibrational inelasticity than that experimentally observed. On the other hand, the angular dependence of each inelastic process is correctly given by our calculations (i.e. the inelasticity increases with the scattering angle), while the excitations with $v'=2$ and 3 are larger than experiments and therefore cause the marked decrease of the $(0\rightarrow 0)$ elastic probability as $\theta_{\text{c.m.}}$ increases. The fact that the $v'=1$, 4, and 5 final states are again in good accord with experiments suggest that the physical energy spacings in O_2^+ may not be well described by either our adiabatic expansion or by the simple harmonic oscillator (HO) spacing used by the experiments.

The individual CT channels shown in Fig. 6, on the other hand, exhibits a closer agreement with the measured data and appear to be better described in the present calculations than in the earlier computations of Ref. 21. The figure reports the individual relative probabilities for each of the final vibrational states in the charge-transfer channel. The open circles are the present results, while the solid ones are the experimental data from Ref. 1. The calculated quantities of Ref. 21 are also shown by the crosses.

The following considerations can be made when examining the data in the figure:

(i) All the inelastic processes given by the present calculations follows very closely the experimental behavior. Contrary to what was obtained from the earlier model-potential calculations,[21] the transitions with larger Δv are not overestimated by the present PES's, which appear to correctly describe both angular behavior *and* relative energy distributions into the various excited vibrational states.

(ii) In the small-angle region, i.e., for scattering into the forward direction, the present calculations produce a marked reduction in the probabilities for the inelastic processes and a dominance of the $(0\rightarrow 0)$ final state, at odds with experiments. As these angular regions are dominated by long-range forces and by the potentials outside the avoided crossings, it appears that the vibrational coupling given there by the present DIM surface is slightly weaker than necessary.

(iii) It is, however, remarkable to observe that the present dynamical calculations and the DIM modeling of the interaction in the $(O_2\text{-}H)^+$ system are capable of reproducing so well the detailed inelastic distributions obtained from the experiments.

As discussed in the previous section, another powerful

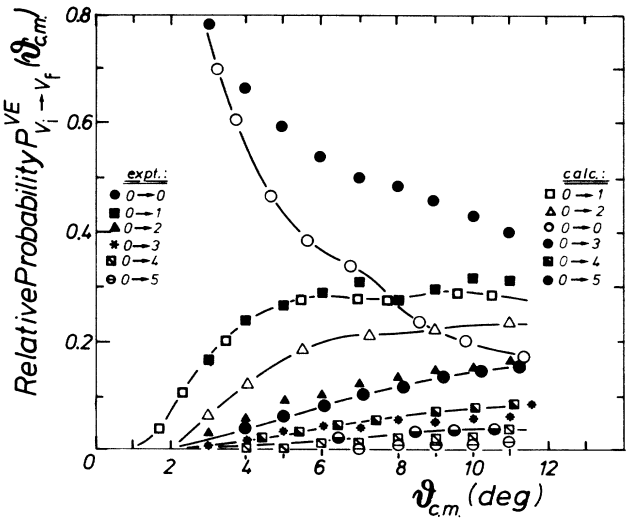

FIG. 5. Relative state-to-state probabilities for the VE channel as functions of the scattering angle. The CT IOSA calculations are given by the curves labeled with the symbols shown on the right side of the figure, while the symbols for the experiments are given on the left side.

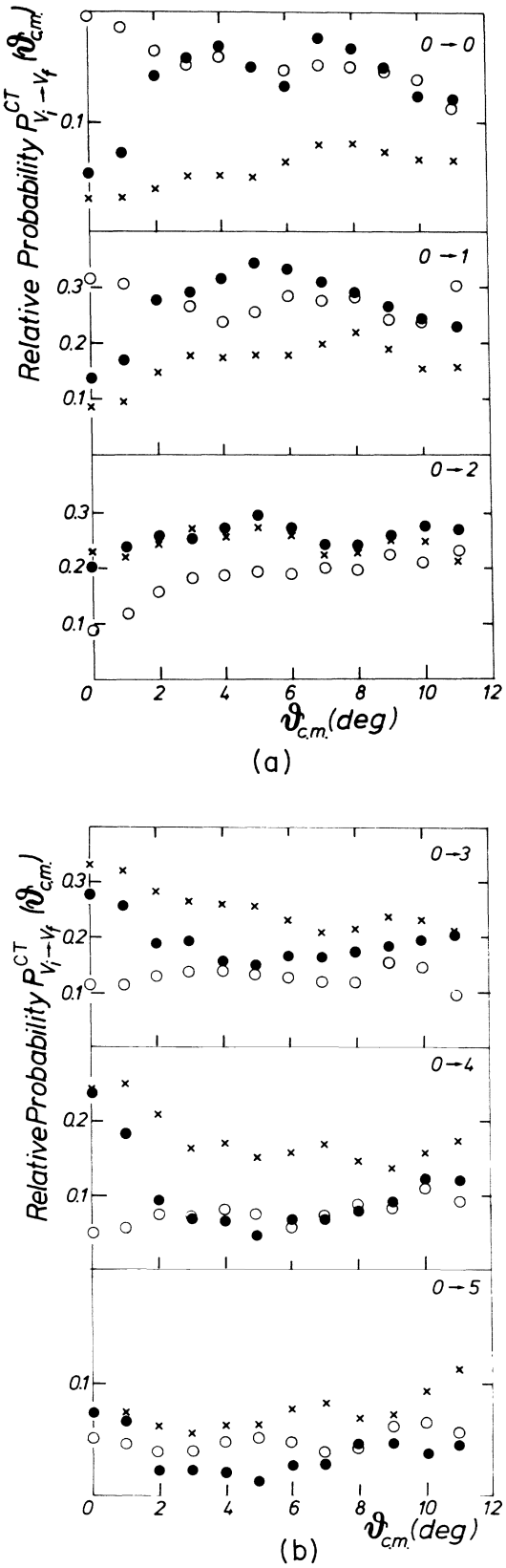

FIG. 6. Relative probabilities for each of the final vibrational states observed in the charge-transfer (CT) channel. The open circles are the present calculations, the solid circles are the experiments from Ref. 1, and the crosses are the calculations from Ref. 21.

way of examining the quality of the calculations is given by the sum of the state-to-state average energy transfers as a function of scattering angle, defined by Eq. (20). The energy spacings between vibrational levels in the O_2 and O_2^+ targets were treated, to be consistent with experiments, as simple harmonic-oscillator spacings, with $h\nu=0.193$ eV for O_2 and 0.233 eV for O_2^+.[1] Thus it becomes a very simple matter to translate the results of Figs. 5 and 6 into the $\Delta E^q(\theta)$ quantity defined in Eq. (20). The comparison with experiments is shown in Fig. 7 for the direct, vibrationally excited VE channel.

The experimental quantities are shown by solid circles and the calculated values are scaled by a factor of 0.66 (shown in the figure) in order to make a better comparison with measurements. The general trend of the average energy transfer is to increase with angle and to extrapolate to a finite, very small value as $\theta\sim 0°$. Within the range of measured distribution, in fact, the ΔE^q value increases by a factor of ~ 2.5. The calculated values turn out to be nearly twice as large as the ones measured, as already indicated by the state-to-state DCS of Figs. 4 and 5, but follow remarkably well the experimental trend:

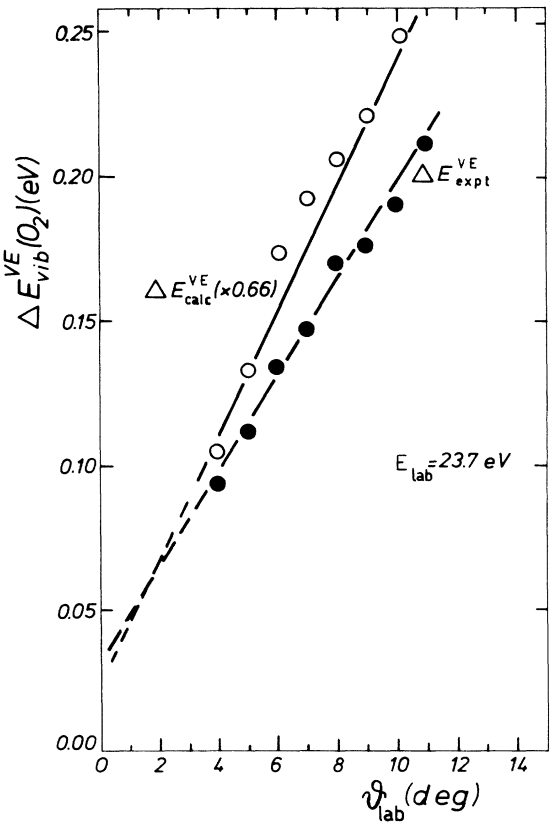

FIG. 7. Computed (open circles) and measured (solid circles) average vibrational energy transfers in the inelastic $H^+ + O_2$ collisions at the stated relative energy. The experiments are from Eq. (1). The computed values have been multiplied by the factor shown in brackets, 0.66.

they increase as θ increases and vary by the same factor of the experiments over the observed range of angles. Thus, one can say that the present DIM surface produces vibrational coupling, which is too strong in the direct channel, but gives a general mapping of the full interaction and of its orientational dependence, which is very close to the one suggested by experiments.

The corresponding results for the charge-transfer channel are presented in Fig. 8, where again the solid circles are the experimental findings and the open circles report the present calculations. In order to make the comparison clearer, the calculated quantities were multiplied by a factor of 1.5 (shown in the figure).

One immediately sees there that the angular dependence is very different, in this channel, from the one shown by the direct process. It is also very different from that expected by Franck-Condon (FC) estimates of the inelastic process.[1] The present calculations therefore confirm the non-FC nature of the vibronic mechanism and exhibit an angular dependence which agrees rather well with measurements, with the exception of the small-angle region already discussed. Moreover, the absolute values for the average energy transfer given by our calculations are smaller than the experiments by a factor which is roughly the inverse of the factor used for scaling the results for the VE channel. Thus, one could simply write that

$$\Delta E^{\rm VE}_{\rm expt}\,\Delta E^{\rm CT}_{\rm expt} \simeq \Delta E^{\rm VE}_{\rm calc}\,\Delta E^{\rm CT}_{\rm calc} \ . \tag{28}$$

One can also note that the above quantities represent a measure of the total relative probabilities of crossing the nonadiabatic region by either hopping at the first passage only or by also hopping at the second passage. In other words, one could qualitatively say that, if one defines

$$\Delta E^{\rm CT} \propto P_{12} \ , \tag{29a}$$

it therefore follows that the other relevant quantity is given by

$$\Delta E^{\rm VE} \propto 1-P_{12} \ , \tag{29b}$$

where P_{12} is the one-way transition probability. Thus, within the simple picture which uses the classical S-matrix approximation[32] one can write the so-called two-way transition probability $\mathcal{P}_{12}$ as given by

$$\mathcal{P}_{12}=4P_{12}(1-P_{12})\sin^2\Delta\varphi \ , \tag{30}$$

where the phase $\Delta\varphi$ is related to the difference of action calculated along the two trajectories from the turning point to the crossing point. If $\Delta\varphi$ is large, then the averaging gives $\langle \sin^2\Delta\varphi\rangle = \frac{1}{2}$, and therefore

$$\mathcal{P}_{12} \simeq 2P_{12}(1-P_{12}) \ . \tag{31}$$

Thus, one could say that our calculations provide a realistic estimate of the $\mathcal{P}_{12}$ quantity for the present system. The latter could be seen as a measure of the overall effect of the nonadiabatic couplings on the vibrational energy-transfer probabilities of *both* channels and a check on the correct overall flux distribution given by our calculations.

As mentioned in the previous section, a further insight into the elementary mechanisms which activate the vibronic inelastic processes could be gleaned from the computed opacities defined in Eqs. (22) and (23). The total opacity sums are shown in Fig. 9 for both channels involved in this system. One clearly sees the marked

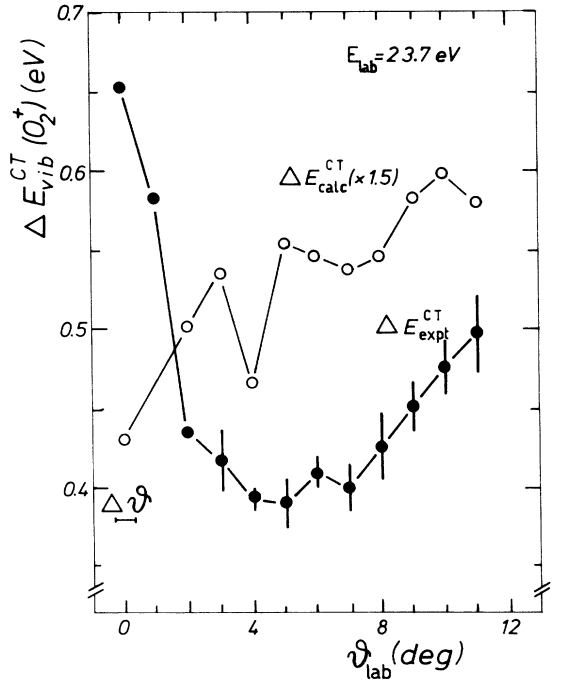

FIG. 8. Same as in Fig. 7 but for the charge-transfer (CT) channel of the collision process. The computed quantities (open circles) are multiplied by a factor of 1.5 for clarity.

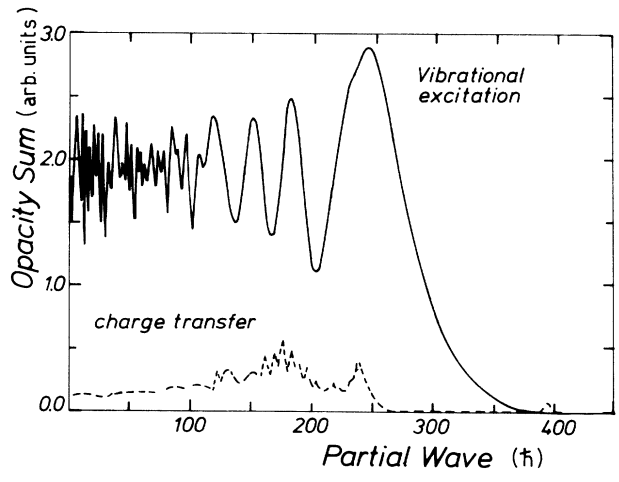

FIG. 9. Computed opacity sums for the VE and CT channels of the present scattering process. The definition of the quantities shown is given by Eq. (23). The data for the CT channel were multiplied by a factor of 5 for clarity.

difference in probability between the two processes and also their differences in behavior as function of angular momentum or partial wave l. In the case of the direct process, in fact, one observes that large contributions to it still occur from the region of impact parameters beyond $l=250$. The latter corresponds to about $4.8a_0$, i.e., to that region of the DIM surfaces where the avoided crossings occur for nearly all the C_s geometries. This means that contributions to the direct process are coming from several trajectories which still do not enter the inner, crossing region of the potential, as they are kept out of it by the corresponding centrifugal barriers. Since the VE process also shows sizeable values of the opacity for the smaller l values, one can argue that in the interaction region between the crossing and the turning point there is still a good number of trajectories which contribute to the direct channel (VE) process.

On the other hand, if one looks at the same quantity for the CT process (dashed line), one sees an entirely different behavior. The probability essentially vanishes beyond the crossing region, i.e., for trajectories which do not enter the inner region between crossings and turning points. Moreover, one sees that within the range of partial waves which sample the inner region, fast oscillations are superimposed on the main opacity structure, indicating the presence of supernumerary rainbows *and* possible Stückelberg oscillations within the interaction region of nonadiabatic coupling.[33]

If now now looks at the results of Fig. 10, i.e., at the partial opacity for each of the individual processes, one discovers another interesting facet of the behavior of the direct, vibrationally inelastic VE channel.

The results shown in the figure refer to the partial opacity defined in Eq. (22) and apply only to the VE process. Similar results for the CT channel have not been shown as they do not alter the analysis already made possible by the opacity sum of Fig. 9. The surprising feature of the individual contributions to the VE channel is that the elastic process, the $(0\rightarrow 0)$ probability, is the *only* one which exhibits contributions beyond the range of impact parameters spanned by the inner region between the turning point and the avoided crossing. All the inelastic processes (two of which are plotted in the figure as examples) show nonvanishing contributions to their relative probabilities only from those trajectories which appear to sample that inner region, i.e., only from trajectories for which the nonadiabatic crossing plays a significant role. As the impact parameters increase beyond the crossing, on the other hand, the corresponding partial waves do not contribute in any important way to the inelastic part of the VE channel. We feel that this is a crucial result from the present calculations, since it allows one to point rather clearly at a specific dynamical mechanism for the vibrational excitation processes which take place during collisions. We will return to this aspect of our findings.

There is now another computed set of quantities which could be usefully employed to extend our understanding of the vibronic process under study. Because of the special way in which each relative proton-molecule orientation is treated by the IOSA dynamics, the present CT IOSA approximation allows us to obtain the various contributions to the inelastic processes as a function of the internal angle γ. In other words, one can obtain from the calculations an orientation-dependent inelastic cross section for either of the q channels, according to the definition of Eq. (24).

The results for the VE and CT processes are shown in Figs. 11 and 12, respectively. In both cases the individual contributions are shown for the various final vibrational states of the vibrational inelastic and vibronic channels. The direct process reported in Fig. 11 indicates a rather weak angular dependence of the excitation mechanism,

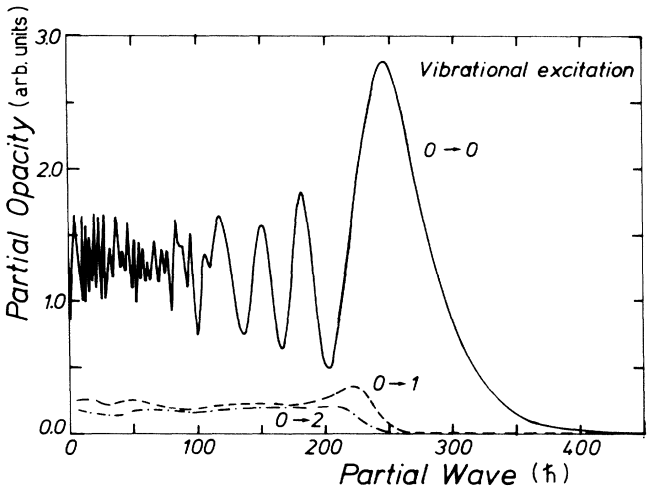

FIG. 10. Computed partial opacity for the direct, vibrationally inelastic VE channel. The inelastic processes shown correspond to the $(0\rightarrow 1)$ and $(0\rightarrow 2)$ transitions of the O_2 molecular target.

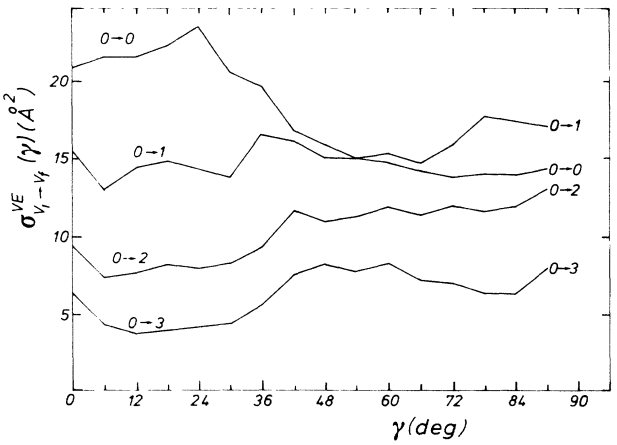

FIG. 11. Computed orientation-dependent partial cross sections for the elastic and inelastic vibrational excitations in the VE channel.

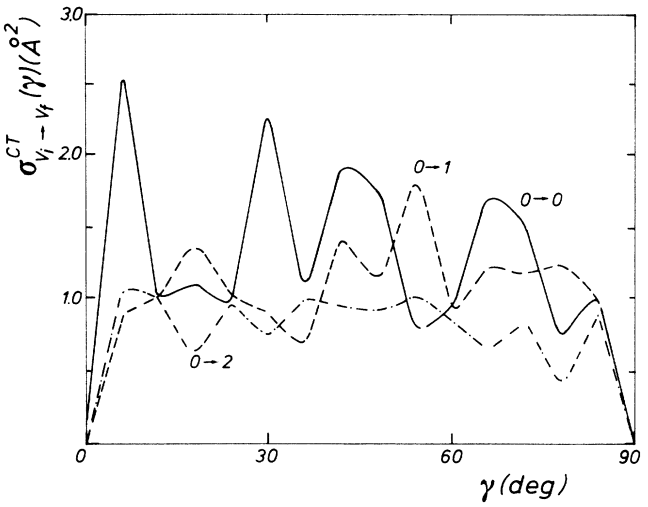

FIG. 12. Same as in Fig. 11 but for the CT channel of the scattering process.

with all orientations playing a very similar role. In other words, it suggests a dominance of the coupling from the inner region for exciting vibrations even in the VE channel, while the specific molecular orientation within it appears to be less important than the nonadiabatic coupling between surfaces. In previous model discussions[14] we surmised that temporary charge-transfer mechanisms cause bond "dilution" or "compression" in either surface and therefore dominate the dynamical coupling between the incoming atom and the molecular bond. The present results confirm quantitatively the above suggestion and further show that such coupling is affected little by molecular orientation when the outgoing products are in the VE channel.

On the other hand, when one observes the same quantity for the CT channel (Fig. 12) one sees that orientational effects are more important: the individual γ-dependent cross sections appear to strongly oscillate as a function of γ, and we find some of the C_s geometries to be more efficient than others in causing the inelastic transition to occur. In this case, one also sees that the CT cross sections vanish for $\gamma=0°$ and 90°, as expected from the fact that the avoided crossings become real crossings in the adiabatic representation at those orientations.

A further useful index of behavior is also given by the relative energy transfers as a function of γ and summed over all final states, as given by Eq. (26). The results of our calculations are shown in Fig. 13 for both channels and essentially confirm the indications of the previous results from the $\sigma^q(\gamma)$: the VE process depends very little on orientation and, in agreement with the experiments, indicates that the amount of energy which is being transferred is lower than that in the CT channel. The latter process, on the other hand, goes abruptly to zero within a narrow polar "cone" corresponding to the C_{2v} and $C_{\infty v}$ orientations. The polar plot shown in the lower part of the figure gives a rather clear graphical presentation of this result and suggests once again that orientational effects, in the present system, play a less important role than that played by the vibronic coupling during the nonadiabatic collisional process.

V. CONCLUSIONS

In the computational treatment discussed in this work, we have analyzed in detail the vibrational excitation processes, which occur during the collisional events listed in Eq. (1), which can be related to both direct scattering (VE) and charge-transfer (CT) scattering encounters.

The interaction potential surfaces involved have been obtained from previous DIM model calculations,[20] and the quantum dynamics with both the potential coupling and vibrational coupling has been treated within the CT IOSA approximation.[12,28]

The final comparison with experimental results, and the analysis of various IOSA-computed intermediate

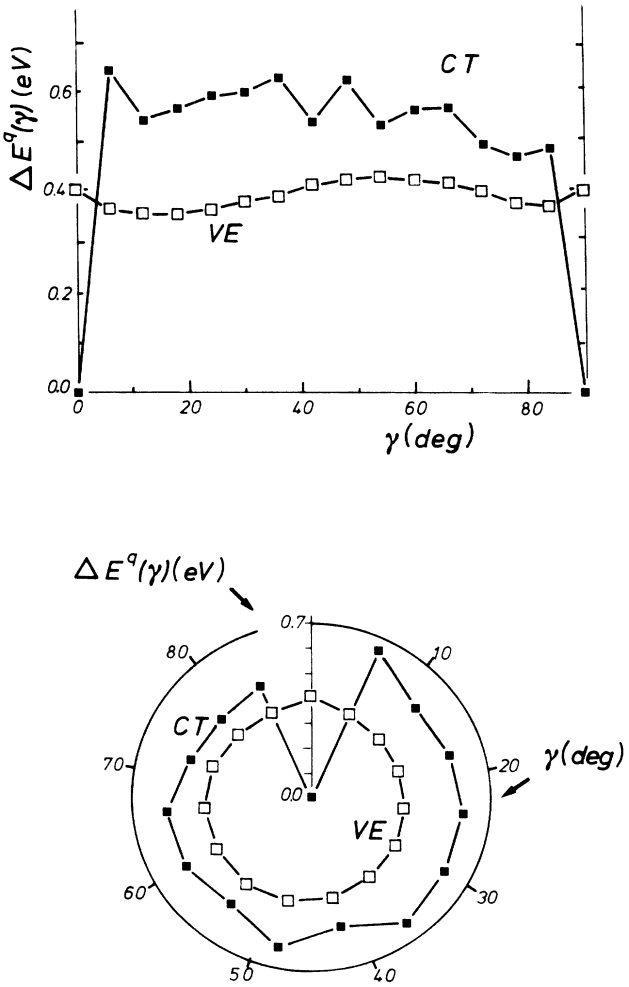

FIG. 13. Average relative energy transfer computed as a function of orientation of both the direct (VE) and the charge-transfer (CT) channels. The top part of the figure shows the results as a function of γ in a Cartesian plot, while the bottom part shows them in a polar plot.

quantities, have shown the following:

(i) The computed total differential cross sections for both channels are in good agreement with experiments and both exhibit the rainbow oscillations which appear in the measurements. Moreover, the individual, state-to-state DCS's are in fair agreement with experiments for the VE channel, but exhibit discrepancies in their relative magnitude with respect to measured values in the CT channel.

(ii) The relative inelastic probabilities in the VE channel follow well the general angular behavior of the corresponding experimental quantities by correctly increasing as the scattering angle increases. The computed transitions with $\Delta v > 1$ are, however, overestimated in magnitude, and indicate a stronger vibrational excitation than that observed experimentally.

(iii) The corresponding relative energy transfers are also produced by the theory in good accord with the experiments as far as their angular dependence is concerned. They turn out to be, however, larger by about 30% with respect to the measured values.

(iv) The CT channel relative probabilities, computed for each of the final vibrational states of O_2^+ which are experimentally observed, turn out to be in very good agreement with measurements in terms of angular dependence and absolute values for transitions down to $\Delta v = 5$. The probabilities for the $\Delta v = 2$ and 3 processes, however, are underestimated by roughly the same amount by which those for the VE channel were overestimated.

(v) As a consequence of the above behavior, the average energy transfer for the CT channel is smaller than the experiments by the same 30%, although it follows closely the angular behavior of the observations.

The test of the chosen PES's therefore indicates that the DIM results have provided a rather reliable description of the proton (atom)-molecule interactions and that the chosen dynamical model has been able to yield nearly quantitative agreement between computed and observed flux distribution during scattering.

Moreover, the analysis of opacity functions and steric factors suggest a fairly clear picture for the physical process: the unusually large vibrationally inelastic cross sections observed in this system are due mainly to coupling between vibrational motion and nonadiabatic interaction. In other words, the "local" charge-transfer picture of the $(O_2\text{-}H)^+$ complex which occurs inside the avoided crossing volume is mostly responsible for releasing electronic energy into vibrational modes in *both* the outgoing channels observed experimentally.

We feel also that the present calculations, which involve *ab initio* modeling of both the interaction and the dynamics, are one of the first examples in which nonadiabatic molecular collision theory is applied to a realistic many-electron system with a good measure of success, and reproduces experiments to a very high level of detail.

ACKNOWLEDGMENTS

Several people have been involved in the many discussions that we have had on the present problem. We therefore thank Peter Toennies, Gereon Niedner-Schatterburg, and M. Noll for many helpful comments on the results and on our understanding of the experiments. Victor Sidis, Franck Schneider, and L. Zülicke have also clarified several aspects of the problem. Last but not least, one of us (F.A.G.) would like to thank the Von-Humboldt-Stiftung for financial support to visit the Göttingen laboratory, where the experiments were first done. Finally, research grants from the Italian Ministry of Education (MPI) and the Italian National Research Council (CNR) are also acknowledged.

[1]M. Noll and J. P. Toennies, J. Chem. Phys. **85**, 3313 (1986).
[2]U. Gierz, M. Noll, and J. P. Toennies, J. Chem. Phys. **83**, 2259 (1985).
[3]F. A. Gianturco, U. Gierz, and J. P. Toennies, J. Phys. B **14**, 667 (1981).
[4]G. Niedner, M. Noll, J. P. Toennies, and Ch. Schlier, J. Chem. Phys. **87**, 2685 (1987).
[5]B. Friedrich, G. Niedner, M. Noll, and J. P. Toennies, J. Chem. Phys. **87**, 5256 (1987).
[6]See, e.g., M. Noll and J. P. Toennies, in *Collision Theory for Atoms and Molecules*, edited by F. A. Gianturco (Plenum, New York, 1989), p. 401.
[7]M. Baer, R. Düren, B. Friedrich, G. Niedner, M. Noll, and J. P. Toennies, Phys. Rev. A **36**, 1063 (1987).
[8]See, e.g., J. C. Tully, in *Dynamics of Molecular Collisions, Part B*, edited by W. M. Miller (Plenum, New York, 1976), p. 217.
[9]E. Bauer, E. R. Fisher, and F. R. Gilmore, J. Chem. Phys. **51**, 4173 (1969).
[10]A. Bjerre and E. E. Nikitin, Chem. Phys. Lett. **1**, 179 (1967).
[11]J. C. Tully and R. K. Preston, J. Chem. Phys. **55**, 562 (1971).
[12]M. Baer, G. Niedner-Schatteburg, and J. P. Toennies, J. Chem. Phys. **91**, 4169 (1989).
[13]R. K. Preston and J. C. Tully, J. Chem. Phys. **54**, 4297 (1971).
[14]V. Staemmler and F. A. Gianturco, Int. J. Quantum. Chem. **28**, 553 (1985).
[15]F. Schneider, L. Zülicke, F. Di Giacomo, F. A. Gianturco, I. Paidarová, and R. Polak, Chem. Phys. **128**, 311 (1988).
[16]F. Schneider and R. J. Gdanitz (unpublished results).
[17]J. Vojtik, Int. J. Quantum Chem. **28**, 943 (1985).
[18]D. Grimbert, B. Lassier-Govers, and V. Sidis, Chem. Phys. **124**, 187 (1988).
[19]J. C. Tully, J. Chem. Phys. **58**, 1396 (1973).
[20]F. A. Gianturco, A. Palma, and F. Schneider, Int. J. Quantum Chem. **37**, 729 (1990).
[21]V. Sidis, G. Grimbert, M. Sizun, and M. Baer, Chem. Phys. Lett. **163**, 19 (1989).
[22]M. Baer, Chem. Phys. Lett. **35**, 112 (1975); Chem. Phys. **15**, 49 (1976).
[23]F. T. Smith, Phys. Rev. **179**, 111 (1969).
[24]X. Chapuisat, A. Nauts, and D. Dehareng-Dao, Chem. Phys. Lett. **95**, 139 (1983).
[25]M. Baer, in *The Theory of Chemical Reaction Dynamics*, edited by M. Baer (Chemical Rubber, Boca-Raton, FL, 1985), Vol. II, Chap. IV.
[26]M. Baer, G. Drolshagen, and J. P. Toennies, J. Chem. Phys. **73**, 1690 (1980).

[27]K. P. Huber and G. Herzberg, *Constants of Diatomic Molecules* (Van Nostrand, New York, 1979).
[28]M. Baer and H. Nakamura, J. Chem. Phys. **87**, 4651 (1987).
[29]See, e.g., D. C. Clary, J. Phys. Chem. **91**, 1718 (1987).
[30]F. A. Gianturco, A. Palma, and F. Schneider, Chem. Phys. **137**, 177 (1989).
[31]M. Baer, G. Niedner-Schatteburg, and J. P. Toennies, Chem. Phys. Lett. **167**, 332 (1990).
[32]See, e.g., E. E. Nikitin and L. Zülucke, *Theory of Chemical Elementary Processes* (Springer-Verlag, Berlin, 1978).
[33]E. C. G. Stueckelberg, Helv. Phys. Acta **5**, 369 (1932).